GEORG-AUGUST-UNIVERSITÄT GÖTTINGEN

Uploaddatum: 31.08.2025
Uploadzeit: 16:55

Dies ist ein von FlexNow automatisch beim Upload generiertes Deckblatt. Es dient dazu, die Arbeit automatisiert der Prüfungsakte zuordnen zu können.

**This is a machine generated frontpage added by FlexNow.
Its purpose is to link your upload to your examination file.**

Matrikelnummer: 24364994

GEORG-AUGUST-UNIVERSITÄT GÖTTINGEN IN PUBLICA COMMODA SEIT 1737

Fakultät für Physik

Bachelor's Thesis

Untersuchungen der Top-Antitop-Produktion in Verbindung mit einem W-Boson bei $\sqrt{s} = 13.6$ TeV mit ATLAS

Studies of Top-Antitop Production in Association with a W Boson at $\sqrt{s} = 13.6$ TeV with ATLAS

prepared by

Engla Bergqvist

from Stockholm

at the II. Physikalischen Institut

Thesis number:	II.Physik-UniGö-BSc-2025/07
Thesis period:	26th May 2025 until 31st August 2025
First referee:	Prof. Dr. Arnulf Quadt
Second referee:	Apl. Prof. Dr. Jörn Große-Knetter

Abstract

Diese Arbeit analysiert den $t\bar{t}W$-Prozess unter Verwendung des Ansatzes der Legacy-Run-2-Analyse, im Fall von Zwei-Lepton-Gleichzeichen-Events (2lSS) aus Monte-Carlo-Simulationen sowie aus dem zwischen 2022 und 2024 gesammelten Proton-Proton-Datensatz, mit dem Ziel, das Standardmodell weiter zu validieren. Signalregionen und Kontrollregionen werden entsprechend der 2lSS-Selektion definiert, um das Monte-Carlo-$t\bar{t}W$-Signal gezielt zu erfassen und die HintergrundbeitrÃ¤ge einzuschrÃ¤nken. Eine Maximum-Likelihood-Fit sowie ein Asimov-Fit werden auf den Signal- und Kontrollregionen durchgeführt. Der einzige Parameter, der im Fit variieren darf, ist die Signalstärke der Monte-Carlo-$t\bar{t}W$-Stichprobe, was zu einer gemessenen Signalstärke von $\mu(t\bar{t}W) = 1.00 \pm 0.12$ führt, welche das Standardmodell weiter bestätigt.

Stichwörter: $t\bar{t}W$ Prozess, ATLAS, Run 3, 2lSS-Analyse

Abstract

This thesis analyses the $t\bar{t}W$ process, following the approach of the legacy Run 2 analysis, in the case of two-lepton same-sign (2lSS) events from both Monte Carlo simulations and the proton-proton data set collected between 2022 and 2024 with the goal of further validating the Standard Model. Signal regions and control regions are defined, according to the 2lSS selection, to target the Monte Carlo $t\bar{t}W$ signal and to constrain background contributions, respectively. A maximum-likelihood fit and an Asimov fit are performed on the signal regions and control regions. The only parameter allowed to vary in the fit is the signal strength of the $t\bar{t}W$ Monte Carlo sample, which results in a measured signal strength of $\mu(t\bar{t}W) = 1.00 \pm 0.12$, which further validates the Standard Model.

Keywords: $t\bar{t}W$ process, ATLAS, Run 3, 2lSS analysis

Contents

1 Introduction

Humankind has always been curious about trying to understand how things work. From the ancient Greek philosophers to today's physics. A will to explain how everything is built up has always existed. From the view that everything was built up by four elements, namely earth, water, air, and fire, to today's Standard Model of particle physics, where the Standard Model is the most capable theory today.

However, there is still much to explore when it comes to deepening our understanding of particles. One important aspect is measuring rare processes to both deepen our understanding of the Standard Model and test its limitations. The top-antitop production in association with a W boson ($t\bar{t}W$) is one of those. The inclusive $t\bar{t}W$ production cross-section was measured after the LHC Run 2 to be 890 ± 80 fb [1] and now it can be repeated for the Run 3 data.

This thesis is structured as follows: Section 2 describes the Standard Model with a focus on the top quark and the top-antitop production in association with a W Boson, Section 3 describes the ATLAS detector, and Section 4 provides a description of the thesis topic and timeline.

2 Theory

2.1 Standard Model

The Standard Model (SM) of particle physics, containing 17 particles and 3 of the 4 fundamental forces, is presently the most effective theory in particle physics [2–4]. The theory has predicted the existence of many particles, for example, the top quark [4]. The 17 particles are divided into two groups: fermions and bosons (see Fig. 2.1). The 12 fermions are divided into two subgroups, quarks and leptons, and three generations of each [2, 5].

The leptons (ℓ) include, from the lightest/first generation to the heaviest/third generation, the electron (e), muon (μ), tau (τ), and respective neutrino (ν_ℓ), written as (ν_ℓ ℓ) [2].

The quarks (q) are divided into up- and down-types depending on their electric charge, $+2/3\,e$ and $-1/3\,e$, respectively. The up types, from the lightest/first generation to the heaviest/third generation, are up (u), charm (c), and top (t). And, the down types are down (d), strange (s), and bottom (b) [2, 6]. The quarks also carry different colour charges, blue, green, and red, as required by the Pauli exclusion principle when binding three quarks of the same type together [5, 6].

Each fermion has a distinct flavour, and it is almost always conserved, except for the weak interactions through W bosons [7, 8].

There exist 5 bosons: the photon (γ), mediator of the electromagnetic interaction; the W and Z bosons, mediators of the weak interaction; gluons (g), mediators of the strong interaction; and the Higgs boson (H), mediator of the Higgs field [2, 3, 7, 9–11].

Quantum Chromodynamics (QCD) describes how gluons mediate the strong force. Gluons are the carriers of colour charge and are responsible for binding quarks together in such a way that overall colour neutrality is maintained [2, 4–6, 12].

The electroweak force (EWK) unifies the electromagnetic and weak interactions. This unification is achieved through the Higgs mechanism, which gives mass to the W and Z bosons, while the photon remains massless [2, 3, 7–11, 13, 14].

Each particle in the SM has its antiparticle with the opposite quantum numbers. How-

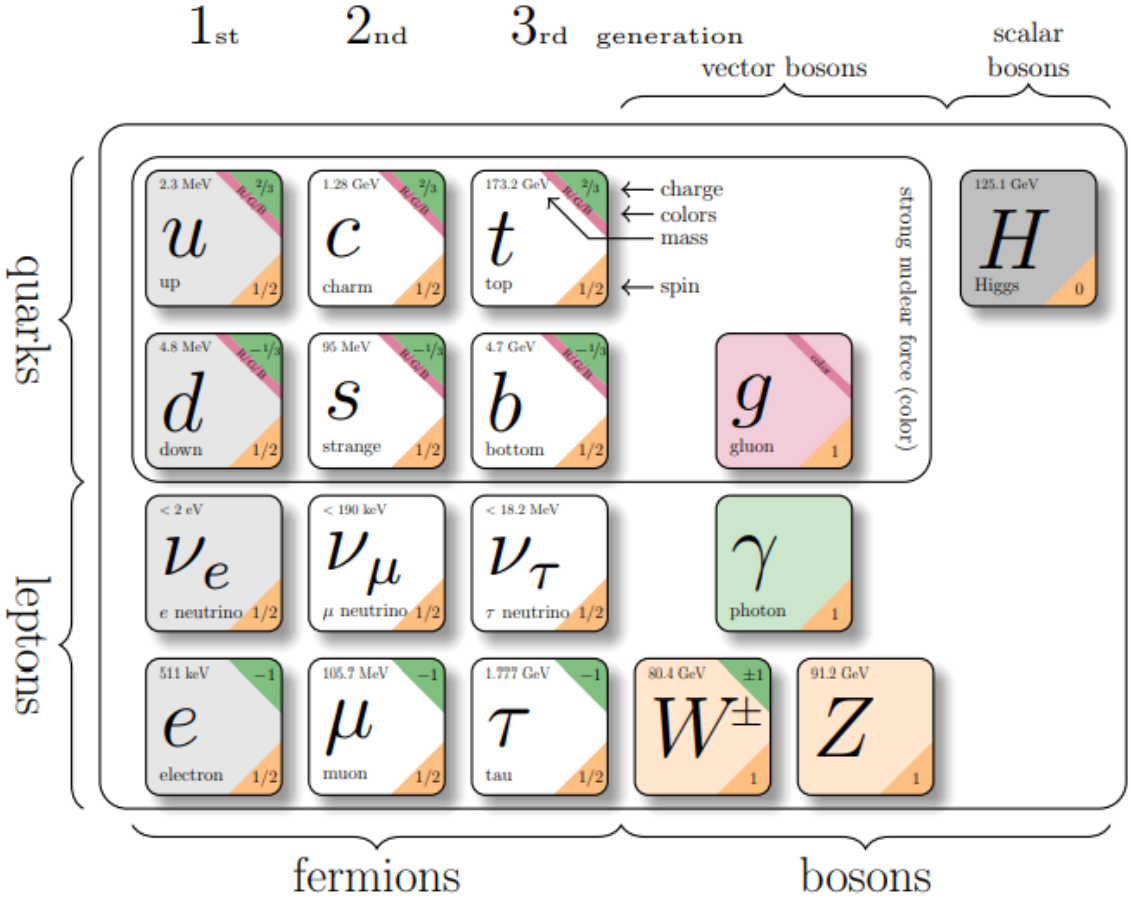

Figure 2.1: Summary of the Standard model [2]

ever, this means that the Z, γ, and H are all their own antiparticles [2, 3].

2.2 Top Quark

The top quark, with a mass of approximately 172.5 GeV, was discovered at the proton-antiproton collider Tevatron in 1995 by the CDF and DØ collaborations [15, 16]. It is the heaviest known elementary particle. Therefore, it has been a subject of many measurements by ATLAS and CMS at the Large Hadron Collider (LHC) [17, 18], both during the so-called Run 1, the first data taking phase at a center-of-mass energy of $\sqrt{s} = 7$ and 8 TeV, and Run 2, the second data taking phase, with $\sqrt{s} = 13$ TeV and now for the third ongoing data taking phase, Run 3, at $\sqrt{s} = 13.6$ TeV.

The main production process of top quarks at a hadron collider is by single-top-quark events through electroweak processes and top-antitop ($t\bar{t}$) pair production via the strong interaction. The production of $t\bar{t}$ pairs is initiated either by quark-antiquark annihilation or by gluon-gluon fusion [19]. In contrast, single top-quark production via the electroweak

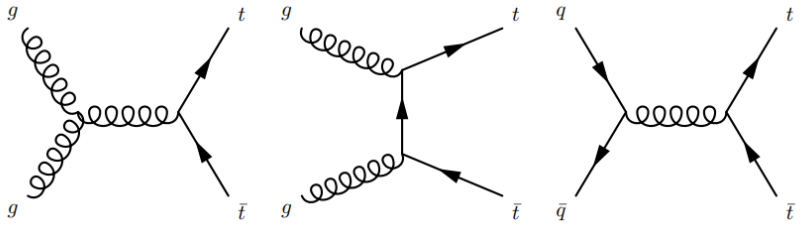

Figure 2.2: Illustrative Feynman diagrams of the $t\bar{t}$ production via strong interaction launched by, gluon-gluon fusion in s-channel (left) and t-channel (middle) or quark-antiquark annihilation (right) [20].

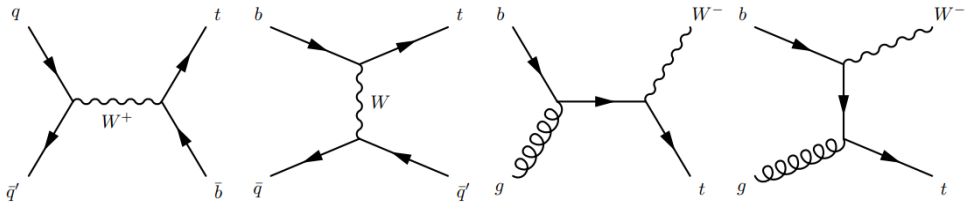

Figure 2.3: Illustrative Feynman diagrams of the single-top-quark production, s-channel (left), t-channel (left-middle) and tW channel (the two to the right) [20].

force occurs primarily through three modes: the t-channel, the s-channel, and the tW channel [19].

The lifetime of the top quark is shorter than the hadronisation time, the time it takes to form a hadron. Therefore, the top quark does not form bound states with other quarks and instead mainly decays into a W boson and a b-quark [19]. The b-quark evolves into a hadronic jet, and the W boson decays either leptonically to a lepton and its neutrino or hadronically to two lighter quarks. This gives rise to three different final states for the $t\bar{t}$ production: the fully hadronic final state, the dilepton final state, and the semileptonic final state [19]. Meanwhile, for the single-top-quark production, the s and t-channel decay into either a fully hadronic or single-lepton final state, and the tW channel can have all three final states [19].

2.3 $t\bar{t}W$ Process

The top-antitop production in association with a W boson, observed in Run 2, is one of the rarest and heaviest processes accessible at the LHC [21, 22]. Among the many SM processes, this is one of the few processes that inherently produce same-sign dilepton pairs. This fact is exploited in searches for rarer processes in SM, because $t\bar{t}W$ is the dominant background [23–25].

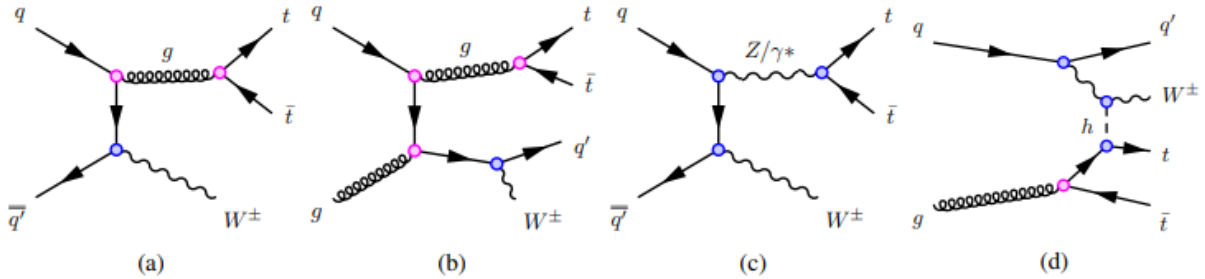

Figure 2.4: Representative Feynman diagrams for the leading productions modes of $t\bar{t}W$, where electroweak couplings(α) correspond to the blue circles and QCD couplings(α_s) correspond to the pink circles. (a) the leading order contribution ($\alpha\alpha_s^2$), (b) next leading order(NLO) contribution ($\alpha\alpha_s^3$), (c) only electroweak contributions (α^3), and (d) a combination of NLO QCD and electroweak contribution ($\alpha^3\alpha_s$) [1].

The $t\bar{t}W$ process can be produced through various mechanisms. It may be initiated by quark-antiquark or quark-gluon interactions via either QCD or electroweak processes, or a combination of both. Figure 2.4 shows the dominant production modes of $t\bar{t}W$, two quark-antiquark and two quark-gluon processes. The leading order (LO) at the initial state of the quark-antiquark process has charge-asymmetric production of $t\bar{t}W^-$ and $t\bar{t}W^+$ due to unusual complex high-order QCD, EWK corrections, and the parton distribution function [26–28]. The EWK correction will consequently enable additional production mechanisms, which are interesting for understanding the SM, such as tW-scattering [29, 30]. Therefore, it is important to observe the $t\bar{t}W$ production for a greater understanding of the SM.

In 2023 the ATLAS Collaboration measured the inclusive $t\bar{t}W$ production cross-section using data from Run 2 to be 890 ± 80 fb compared to the reference theoretical prediction of 722^{+70}_{-78}(scale)$\pm$7(PDF) fb [1].

3 The Large Hadron Collider and ATLAS Detector

One of the frontiers of particle physics is being explored through the physics studied at the ATLAS detector at LHC located at CERN. The Large Hadron Collider (LHC) is a superconducting proton-proton collider, consisting of two rings with a length of 27 km and designed to produce a proton-proton collision with centre-of-mass energy of 14 TeV. This allows detecting rare events [31]. The detection happens in ATLAS, which is built up by an Inner Detector, a Hadronic and an Electromagnetic Calorimeter, and a Muon Spectrometer. The detector components will be introduced in the following sections. A cross-section view of ATLAS is given in Fig. 3.1.

3.1 Inner Detector

The Inner Detector is the first part of ATLAS where the products of the collision are reconstructed, with the main purpose of identifying the tracks and vertices of the charged particles. By doing so, their transverse momentum can be obtained. b-tagging, the process of identifying jets originating from b-quarks, is a key capability of the Inner Detector. Due to the relatively long lifetime of B-mesons in comparison to many other particles produced in high-energy collisions, the B-meson can travel a measurable distance before decaying. When it decays, a vertex occurs, providing a distinctive signature that is later used for particle identification and event reconstruction.

The detector consists of three different parts: the pixel detector, the semiconductor tracker, and the transition radiation tracker.

The pixel detector is the innermost part of the Inner Detector. This is the first detector where the charged particles are tracked. The pixels are made up of four layers of silicon on top of a readout. When a charged particle hits the silicon atoms, the silicon becomes ionized, and a current occurs, which goes to the readout where it gets stored or discarded, depending on the information. The detector contributes to the tracking of charged particles with very high granularity and precision, as near as possible to the interaction point.

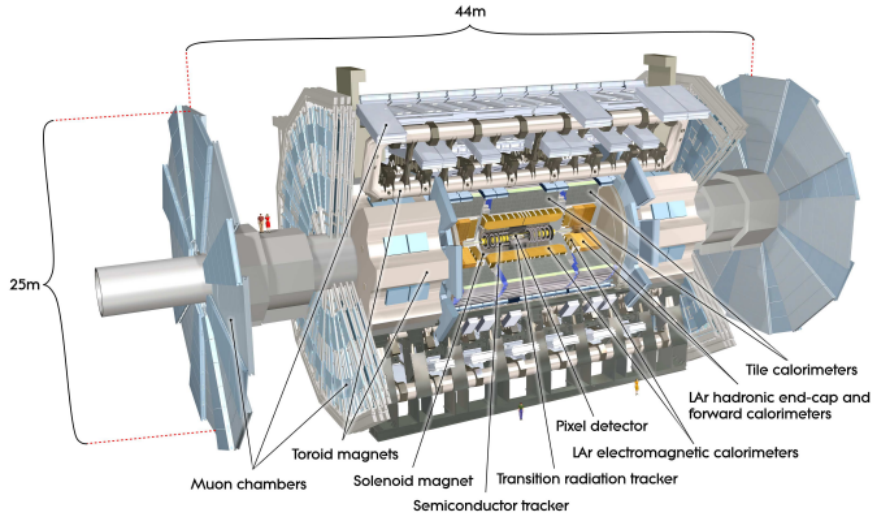

Figure 3.1: An illustration of the ATLAS detector showing the different parts and size of the detector. Where the Muon chambers are the same as the Spectrometer, Pixel Detector, Transition Radiation Tracker, and Semiconductor Tracker, all belong to the Inner Detector, and the Tile calorimeter is a part of the Hadronic Calorimeter. © CERN

This provides results with a good spatial resolution, which is crucial for understanding the trajectories of the charged particles.

The Semiconductor Tracker (SCT) is constructed in a similar manner to the Pixel Detector; however, it uses silicon strips instead of pixels and consists of more stacks. This can later be used to build up the trajectories of the charged particles and complement the pixel detector data.

The transition radiation tracker (TRT) is a gaseous detector built up by multiple straw tubes filled with gas mixtures and has an anode wire on the inside. When a charged particle enters these tubes, it interacts differently with the gas in the tubes by ionization. Therefore, only charged particles interact with the gas, and the main focus is on identifying electrons and their movement. A solenoid magnet is placed around the Inner Detector, which bends the charged particles path. With this information, the momentum can be determined [32].

3.2 Electromagnetic Calorimeter

The Electromagnetic Calorimeter is the next component in ATLAS. It is used to measure the energy of photons and electrons by allowing these particles to pass through alternating layers of passive and active materials. The passive material initiates an electromagnetic

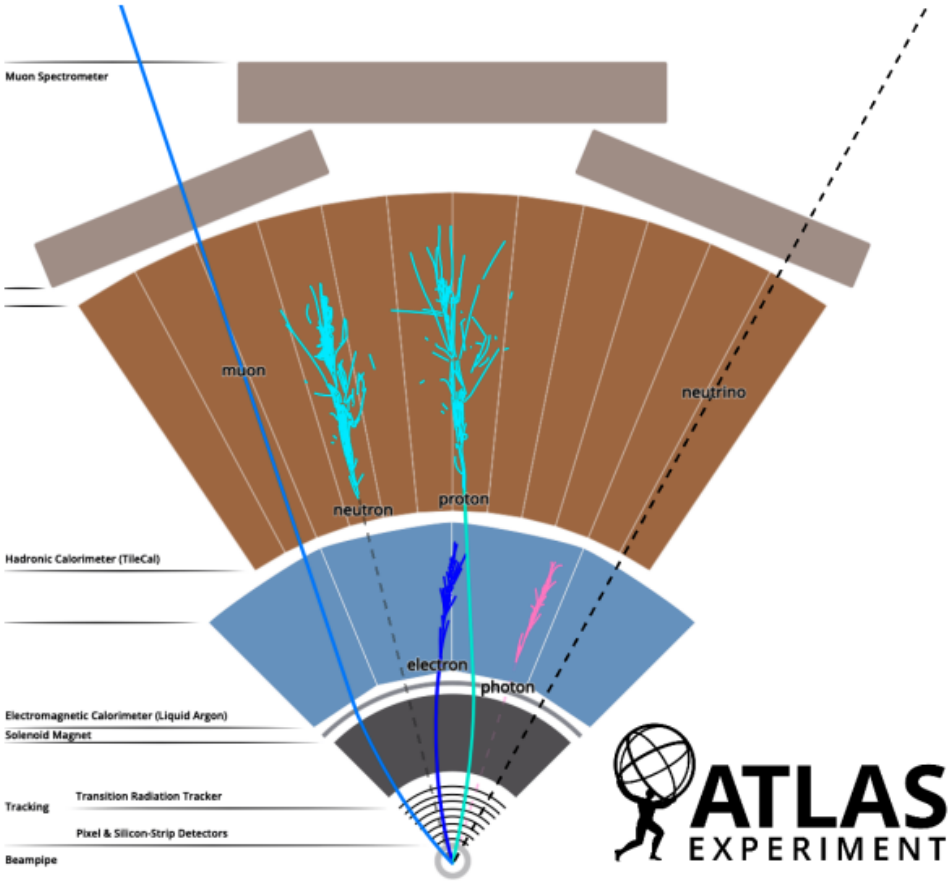

Figure 3.2: A schematic view of a slice of the ATLAS detectors, different layers, and how particles interact with these layers (© CERN). The beam pipe is where the collisions happen, the Inner Detector is the area called tracking.

shower, in which the incoming particle produces secondary particles, leading to a cascade. The active material detects the resulting shower by generating an electrical signal.

This process continues until the showering particles have deposited all their energy and are effectively at rest (see Fig. 3.2). In the ATLAS Electromagnetic Calorimeter, the passive material is lead, while the active material consists of liquid argon. A copper plate is used to collect the resulting electrical signal [33].

3.3 Hadronic Calorimeter

The Hadronic (Tile) calorimeter is the next layer after the Electromagnetic calorimeter of the ATLAS Detector. It is built similarly to the Electromagnetic calorimeter, where the passive medium is steel and the active medium are scintillating plates. The main purpose of the Hadronic calorimeter is to measure the energy of hadrons [34].

3.4 Muon Spectrometer

The Muon spectrometer and the toroidal magnets are the outermost parts of ATLAS. The toroidal magnets are there to bend the path of the muon and, by doing so, enable the measurement of its momentum. The spectrometer also measures the trajectories of the muons [35].

After the muon spectrometer, the transverse energy should be measured to be zero. In many cases, that is not true. There is some missing transverse energy due to the escape of neutrino(s) that ATLAS can not detect [17].

4 Object Definitions

This analysis uses the proton-proton data set collected between 2022 and 2024, and simulated events created using Monte Carlo (MC) generators. The MC events were $t\bar{t}W$, $ttll$, $t\bar{t}H$, VV, tWZ, tW, tZq, $Z + jets$, and $t\bar{t}$, which were later grouped into the samples: $t\bar{t}W$, $ttZ/\gamma*$, $t\bar{t}H$, DiBoson, Others, and Fakes.

4.1 Leptons

In this analysis, two identification levels were used, the Loose and Tight, for both electrons and muons. The tight selection applies stricter requirements on track quality, isolation, and impact parameters to reduce contamination from misidentified hadrons and non-prompt leptons.

Events were further classified using the Loose-not-Tight category, which contains leptons that pass the loose selection but fail the tight criteria. This category is used specifically for the control regions in Sec. 5.2 to get a better understanding of the background events.

4.2 Jets

The jets were put through the baseline criteria of $p_T > 20$ GeV and $|\eta| < 2.5$. A Jet Vertex Tagger criterion was also applied to the jets, assuring real jets from the pile-up jets.

4.3 B-Jets

The main b-jet working point efficiencies used in this analysis are 65% and 77%, which were decided by the jet-flavour-tagging algorithm GN2v01. This was used to then identify the b-jets. In the previous Run 2 analysis ([1]), the legacy results were obtained using 60% instead of 65%, which provided higher purity but lower efficiency than this analysis. In contrast, using a 65% instead of 60% increases the number of selected b-jets.

Table 4.1: A summarised table of the systematic uncertainties.

	Uncertainty %
Luminosity	1.9
$ttZ/\gamma*$	6
$t\bar{t}H$	26
DiBoson	30
Others	50
Fakes	50

4.4 Prompt and Non-Prompt leptons

In the analysis, it is important that the leptons are prompt, or in other words, well isolated, ensuring that the lepton originates from the hard interaction. The truth-classification tool IFFClass was used in the analysis to separate between prompt and non-prompt leptons and classify them. All the samples, except the Fakes, were required to have two prompt leptons. The Fakes containing the $t\bar{t}$ and $Z + jets$ events were divided into four more prominent samples. Two from heavy-flavoured leptons, one for electrons and one for muons, requiring one lepton to originate from a heavy-flavour decay, defining the samples HFel and HFμ. One from a misidentified electron charge, where one of the lepton charges has accidentally been flipped, giving the sample QMisID. The analysis does not take the charged-flipped muons into account, which the legacy ([1]) did not do either. Lastly, the sample OtherFakes, containing events from prompt photon-conversions, electrons from muons, tau decays, light-flavour decay, double fake leptons, known-unknown leptons, and unknown leptons.

4.5 Missing Transverse Energy

Missing transverse energy (MET) is the negative vector sum of the transverse momenta of all reconstructed objects in the event. It provides a measure of momentum imbalance in the plane perpendicular to the beam direction and is sensitive to the presence of non-interacting particles such as neutrinos, which escape the detector without depositing energy. The MET is important for the analysis because the W boson decays into a lepton and a neutrino.

4.6 Systematic Uncertainties

The systematic uncertainty on the luminosity in Run 3, used in the analysis, was estimated to be $\pm 1.9\%$. The theoretical systematic uncertainties for the MC samples were estimated to be $\pm 6\%$ for the $ttZ/\gamma*$, $\pm 26\%$ for the $t\bar{t}H$, $\pm 30\%$ for the DiBoson, and $\pm 50\%$ for the Others and all the samples belonging to the Fakes, see Tab.4.1.

5 Event Selection

This analysis studies two-lepton same-sign (2lSS), events and investigates both through signal regions (SRs) and control regions (CRs). The CRs are where the background should shine clearly over the $t\bar{t}W$ signal, more details are shown in Sec.5.2. The SRs are where the $t\bar{t}W$ signal is supposed to be found by adding extra criteria, see Sec. 5.1 for more details.

Table 5.1: The 2lSS SRs used in the analysis are defined. Here Q is the charge, i stands for leading (i = 0) and subleading (i = 1), and SF stands for same-flavour.

	2lSS (++ or $--$)
number of leptons (i.e e or μ)	= 2 (both passing Tight)
$\Sigma_{l,i}Q$	± 2
Lepton p_T	$p_{T,i} > 20$ GeV
Jet multiplicity	≥ 2
b jet multiplicity	1 at 65% OR at least 2 at 77%
Invariant mass cuts	$m_{ll} > 12$ GeV for SF pairs

Table 5.2: Summary of the total of 24 2lSS SRs.

$2\ell SS$	
$\mu^+\mu^+$, 3j	$\mu^-\mu^-$, 3j
$\mu^+\mu^+$, 4j	$\mu^-\mu^-$, 4j
$\mu^+\mu^+, \geq$ 5j	$\mu^-\mu^-, \leq$ 5j
μ^+e^+, 3j	μ^-e^-, 3j
μ^+e^+, 4j	μ^-e^-, 4j
$\mu^+e^+, \leq$ 5j	$\mu^-e^-, \leq$ 5j
$e^+\mu^+$, 3j	$e^-\mu^-$, 3j
$e^+\mu^+$, 4j	$e^-\mu^-$, 4j
$e^+\mu^+, \leq$ 5j	$e^-\mu^-, \leq$ 5j
e^+e^+, 3j	e^-e^-, 3j
e^+e^+, 4j	e^-e^-, 4j
$e^+e^+, \leq$ 5j	$e^-e^-, \leq$ 5j

Table 5.3: The 2lSS CRs used in the analysis. Here Q is the charge, i stands for leading (i = 0) and subleading (i = 1), and M_T is the transverse mass consisting of all the leptons and the missing transverse energy (MET). The TL, LT, and LL regions are split into two channels: muon ($\mu\mu$ or $e\mu$) and electron (ee or μe) channels.

	2lSS HF
numbers of leptons (i.e e or μ)	$= 2$
PLIV WPs	TL or LT or LL
$\Sigma_{l,i}Q$	± 2
Lepton p_T	$p_{T,i} > 20$ GeV
Jet multiplicity	≥ 2
b jet multiplicity	1 at 77%
Additional cuts	M_T(all l,MET) < 250 GeV

5.1 Signal Regions

The two-lepton same-sign (2lSS) signal regions (SRs) were defined, similarly to the legacy analysis ([1]), using the selection criteria in Tab. 5.1, which enhances the $t\bar{t}W$ signal. The analysis studies the 2lSS events, where the W boson decays leptonically and one of the top quarks decays leptonically, and the other one decays hadronically. This results in two leptons with a net charge of ± 2 and four jets, two of which are b-jets. Requiring both leptons to pass the tight selection criteria further enriches the $t\bar{t}W$ signal.

The SRs were divided into a total of 24 regions according to lepton charge and jet multiplicity, as shown in Tab. 5.2, surrounding the possibilities of having 3, 4, or more than 5 jets in total. This allows the analysis to capture the typical jet configurations expected from the $t\bar{t}W$ process, including cases with missing or additional jets.

5.2 Control Regions

The control regions (CRs) are used to gain a better understanding of the background. Therefore, by loosened up the 2lSS criteria, both that the leptons do not need to be tight and that the number of jets and b-jets is less defined, provides a strong background-enriched sample with little or no contribution from the $t\bar{t}W$ signal.

The CRs are divided into 6 2lSS heavy flavour (HF) regions. Each region belongs either to the muon channel ($\mu\mu$ or $e\mu$) or the electron channel (ee or μe). The leptons need to be either "Tight" (T) or "Loose not Tight" (L), giving three combinations TL, LT, and LL for each lepton channel. The other selection criteria for the CRs are shown in Tab. 5.3.

6 Results

The data and MC samples were subjected to a maximum-likelihood fit, performed over both the CRs and SRs to constrain background contributions and extract the signal strength of the $t\bar{t}W$ process. The signal strength was the only parameter that was adjusted in the fit. In addition, an Asimov fit was performed. This resulted in a signal strength of $\mu(t\bar{t}W) = 1.00 \pm 0.12$, a relative uncertainty of 12%.

In the following sections, more detailed information on the post-fit results is provided.

6.1 Signal Regions

The post-fitted SRs are seen in the Fig. 6.1, 6.2, 6.3, and 6.4. The four figures corresponds to the ee, $\mu\mu$, $e\mu$, and μe channels, where the events are plotted as a function of the number of b-tagged jets with a 77% tagging efficiency. The plots indicate that almost all events have either one or two tagged b-jets.

6.2 Control Regions

The CR plots are shown in Fig. 6.5 and 6.6, which contain three plots for the electron and the muon channels, respectively. The total number of events in the CRs is plotted as a function of the subleading lepton transverse momentum (p_T) in GeV, and binned into two intervals with edges at [20,30,100].

6.3 Pie Charts

The pie charts in Fig. 6.7 show which background MC sample has the largest impact on each CR and SR. The main contributions come from leptons originating from heavy-flavour decays, as well as the OtherFakes sample, which contains various types of non-prompt leptons.

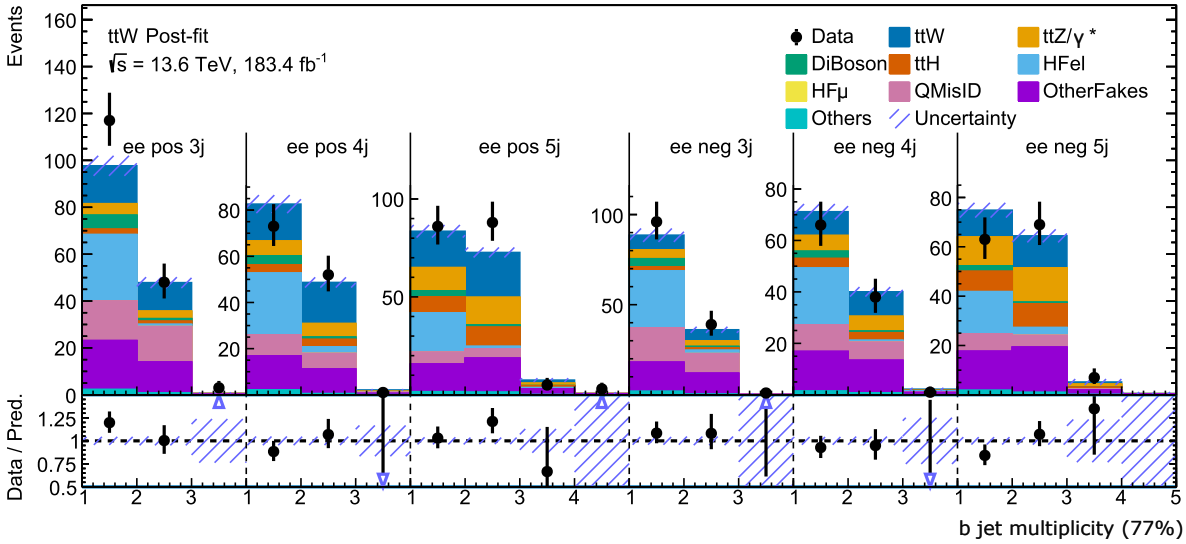

Figure 6.1: 2lSS SRs for the case when the leptons are either two electrons or positrons. The events are plotted over the b jet multiplicity, where the b-jet needs to belong to the 77%.

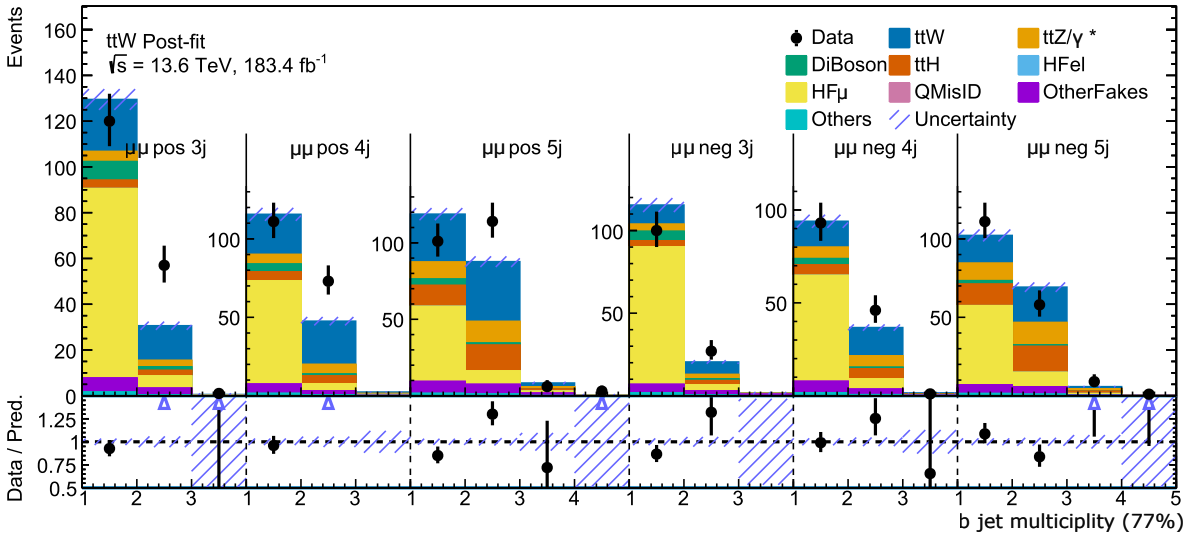

Figure 6.2: 2lSS SRs for the case when the leptons are either two muons or ant-muons. The events are plotted over the b jet multiplicity, where the b-jet needs to belong to the 77%.

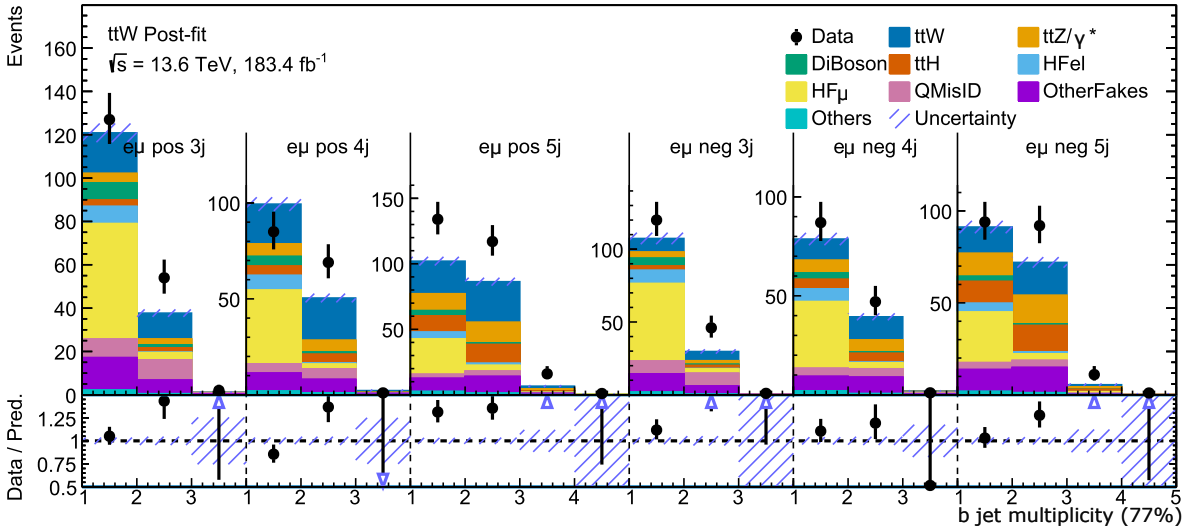

Figure 6.3: 2lSS SRs for the case when the leptons are one leading electron or positron, and one subleading muon or anti-muon. The events are plotted over the b jet multiplicity, where the b-jet needs to belong to the 77%.

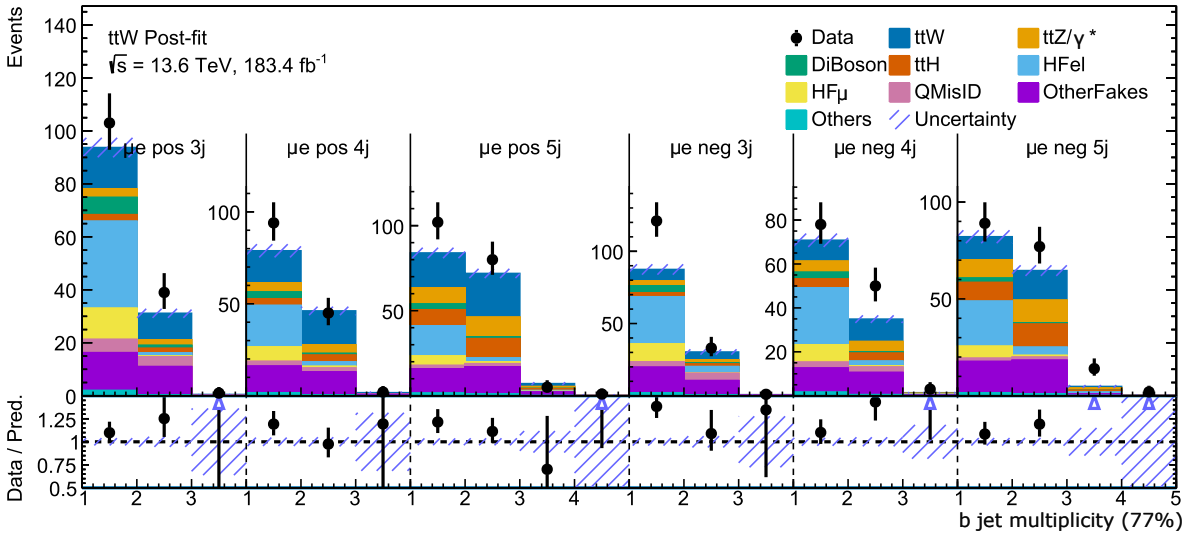

Figure 6.4: 2lSS SRs for the case when the leptons are one leading muon or anti-muon, and one electron or positron. The events are plotted over the b jet multiplicity, where the b-jet needs to belong to the 77%.

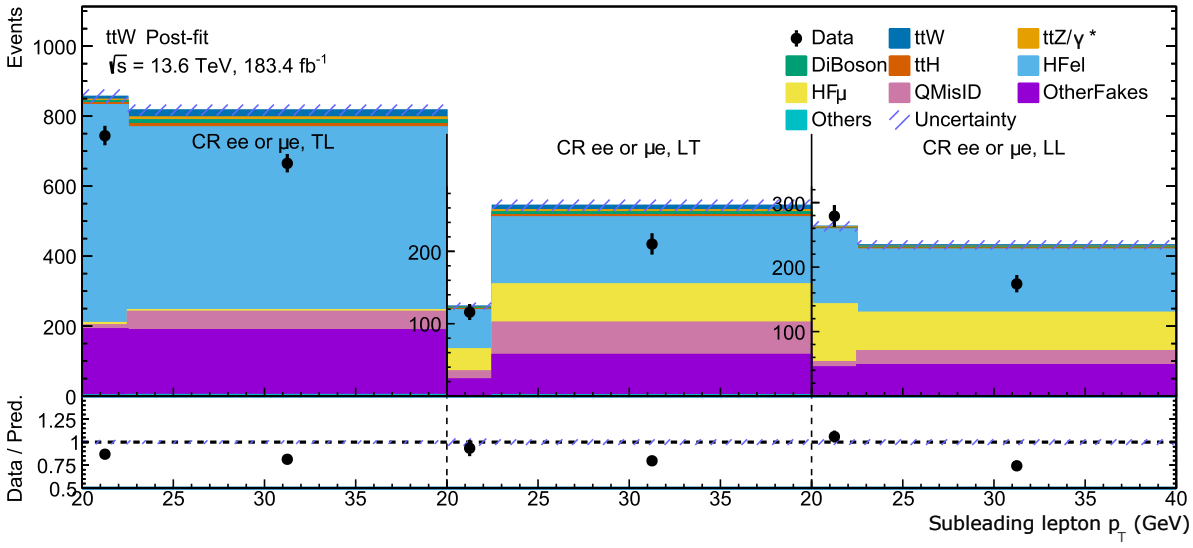

Figure 6.5: CR for 2lSS for the electron channel. The events are plotted over the subleading lepton, the electron, p_T in GeV.

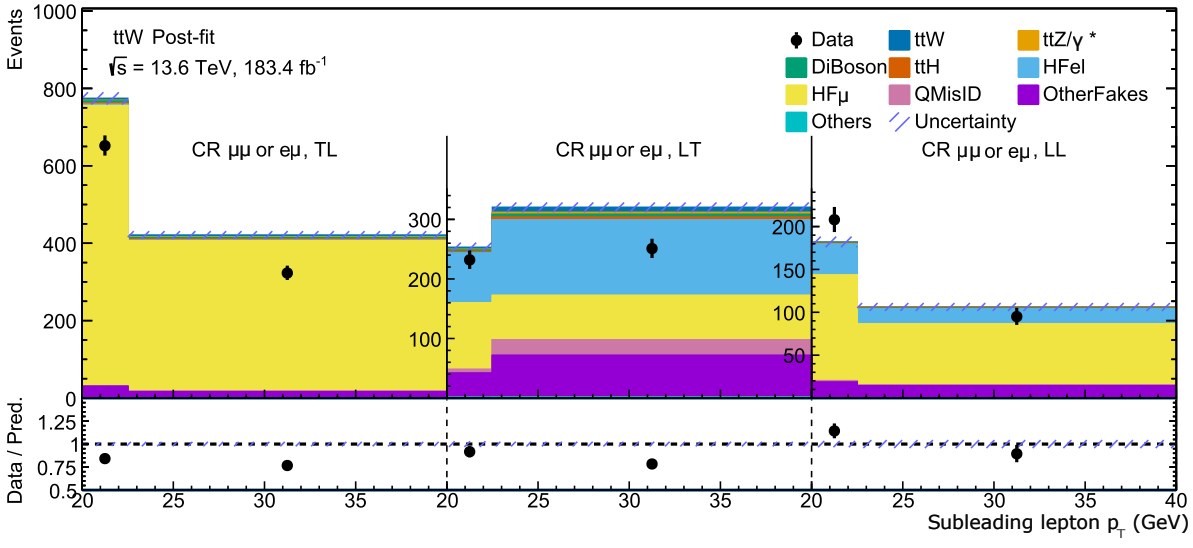

Figure 6.6: CR for 2lSS for the muon channel. The events are plotted over the subleading lepton, the muon, p_T in GeV.

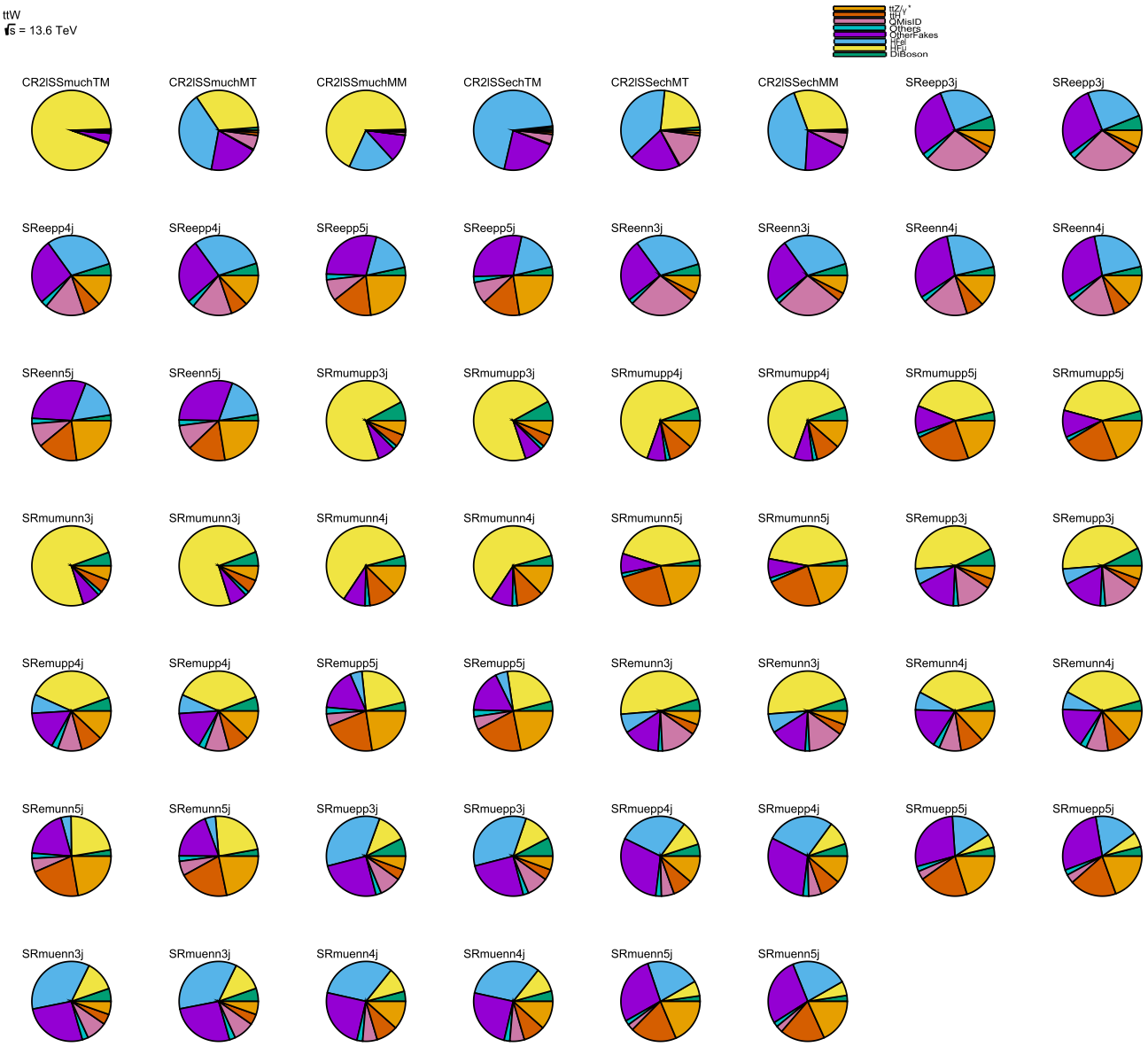

Figure 6.7: Pie-charts over the background samples - $ttZ/\gamma*$ (light-orange), $t\bar{t}H$ (dark-orange), QMisID (pink), Others (turquois), OthersFakes (purple), HFel (light-blue), HFμ (yellow) and DiBoson (green-blue).

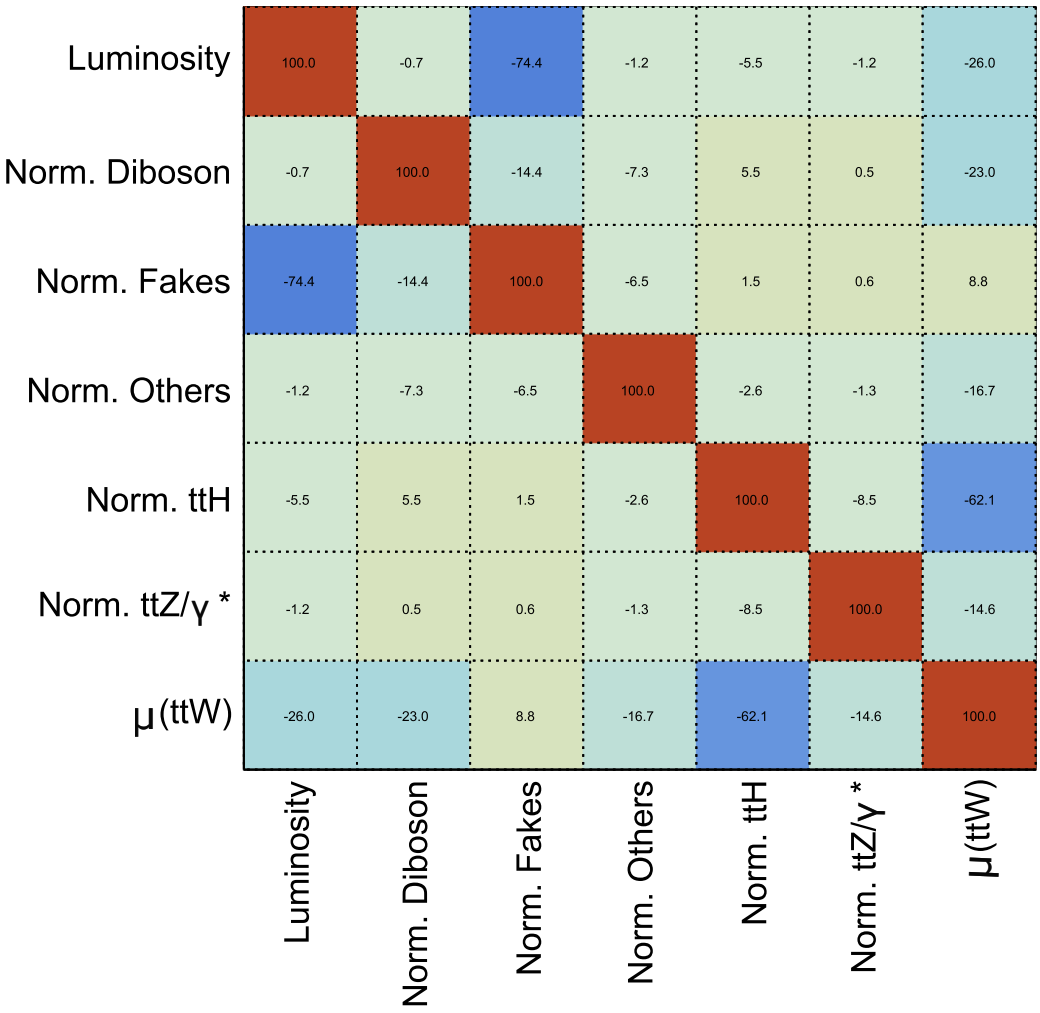

Figure 6.8: Correlation matrix of the fit shows the correlations between the luminosity, the signal strength parameter $\mu(t\bar{t}W)$, and the normalisation factors (NFs) of the main background processes.

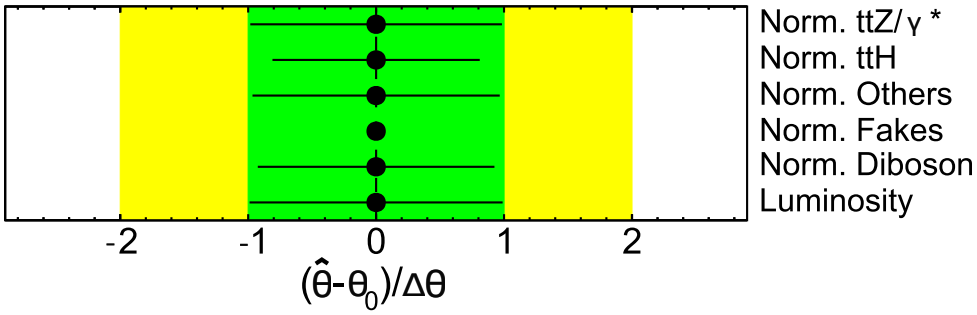

Figure 6.9: Pull plot for the NFs (theoretical systematic uncertainties) and the luminosity (instrumental systematic uncertainties).

6.4 Correlation Matrix

The correlation matrix, shown in Fig. 6.8, displays the correlations between the normalisation factors (NFs) of the main background processes, the luminosity, and the signal strength. Complete correlation occurs between identical parameters, while the remaining values show either a very low correlation or a strong anti-correlation.

6.5 Pull Plot

The pull plot is shown in Fig. 6.9. All the NFs and the luminosity are at or near zero, indicating that none, or almost none, were significantly pulled. The plot also demonstrates that the systematic uncertainties are reasonable.

6.6 Ranking of Nuisance Parameters for the Signal Strength

The ranking of the nuisance parameters (NPs) for the signal strength is shown in Fig. 6.10, which breaks down which parameter uncertainties have the largest relative impact on the signal strength. The top five parameters correspond to the systematic uncertainties, indicating that the systematic uncertainty has a greater impact on $\mu(t\bar{t}W)$ than the statistical uncertainties.

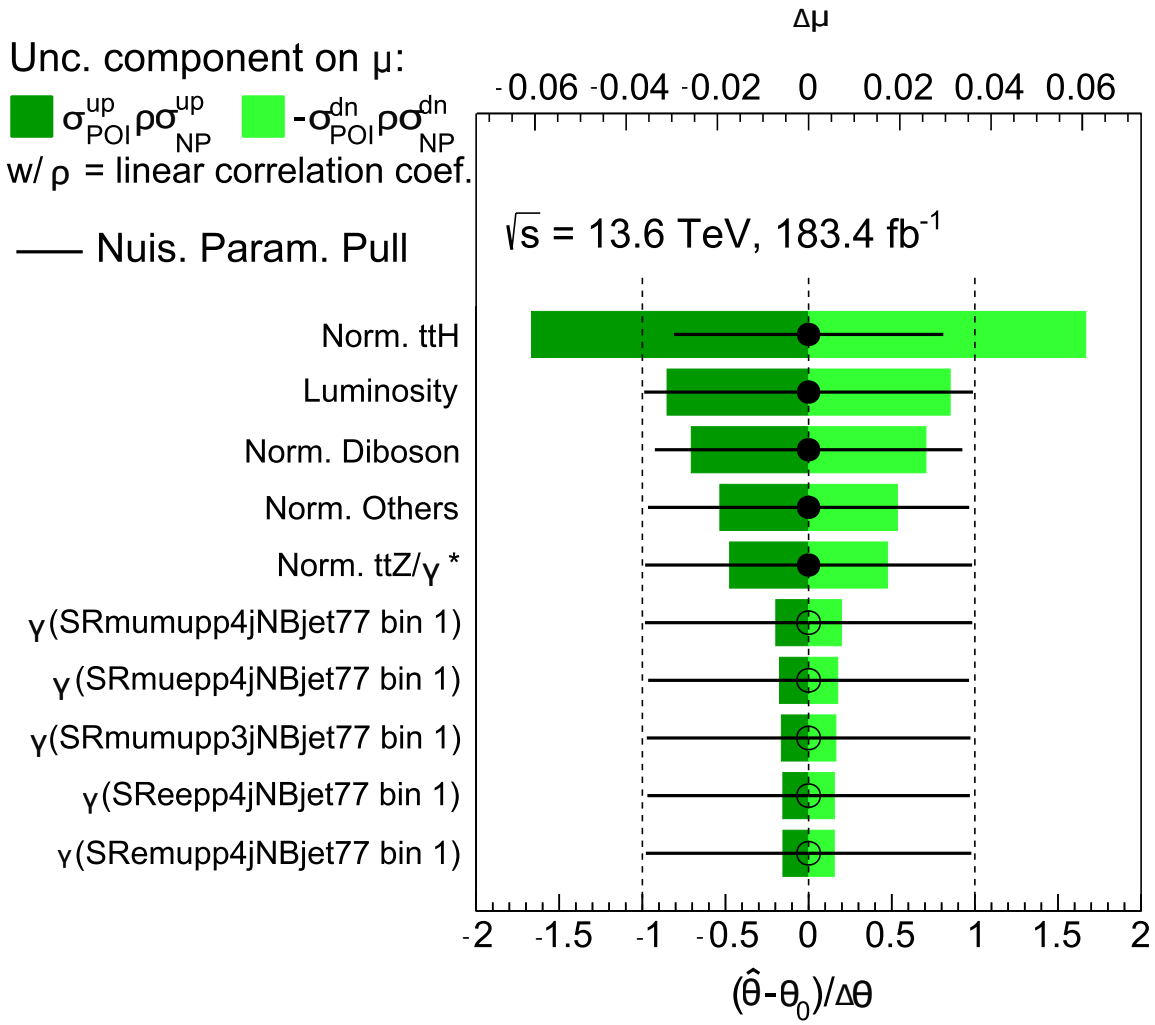

Figure 6.10: Ranking of nuisance parameters (NPs) for the signal strength parameter $\mu(t\bar{t}W)$. The plot illustrates the relative impact of each source of uncertainty on the fitted value of $\mu(t\bar{t}W)$. Both the systematic uncertainties (the NFs and the luminosity, the five biggest), and the statistical uncertainties (the γ:s). The length of each bar corresponds to the change in $\mu(t\bar{t}W)$ when the associated NP is varied within its post-fit uncertainty.

7 Summary and Conclusions

7.1 Summary

This thesis analysed the $t\bar{t}W$ process, following the approach of the legacy Run 2 analysis, in the case of two-lepton same-sign (2lSS) events from both Monte Carlo (MC) simulations and the proton-proton data set collected between 2022 and 2024. Signal regions (SRs) and control regions (CRs) were defined, according to the 2lSS selection, to target MC $t\bar{t}W$ signal and to constrain background contributions, respectively. A maximum-likelihood fit and an Asimov fit were performed to the SRs and CRs. The only parameter allowed to vary in the fit was the signal strength of the $t\bar{t}W$ MC sample, which resulted in a measured signal strength of $\mu(t\bar{t}W) = 1.00 \pm 0.12$.

7.2 Conclusion

The measured signal strength is exactly $\mu(t\bar{t}W) = 1.00$, indicating excellent agreement with the Standard Model (SM) prediction. The relative uncertainty for the $\mu(t\bar{t}W)$ of 12% is relatively small, resulting in a precise measurement. This suggests that further investigations of the $t\bar{t}W$ process are expected to remain highly compatible with the SM, thereby confirming the theoryâs robustness.

This analysis employed a simplified fit in which the signal strength was allowed to vary freely. Consequently, a direct comparison between the SM prediction and $\mu(t\bar{t}W)$ is possible, as the signal strength is not influenced by variations in other parameters. Had $\mu(t\bar{t}W)$ deviated significantly from 1.00, the SM prediction would not agree with the measurement. However, the measured value of $\mu(t\bar{t}W) = 1.00 \pm 0.12$ demonstrates consistency with the SM predictions.

The Asimov fit further supports the SM predictions by estimating the expected uncertainty of the signal strength under the assumption that the SM is correct. The observed $\mu(t\bar{t}W)$ and its small uncertainty confirm that the data are in very good agreement with the SM.

Finally, the systematic uncertainties remain the dominant contribution to the uncer-

tainty on $\mu(t\bar{t}W)$, as shown in Fig. 6.10. Reducing these systematic uncertainties in future measurements could lead a more precise determinations of the signal strength, futher strengthening the validation of the SM.

7.3 Further Studying of the $t\bar{t}W$ Process

The legacy provided a more detailed investigation of the $t\bar{t}W$ process ([1]). Fully reproducing this analysis would offer a deeper and more reliable understanding of the process, benefiting from the repetition of the study. Two examples highlight the added value of the legacy approach.

First, the legacy analysis included events in which $t\bar{t}W$ decayed into three leptons (3l). This decay channel was explored in the current analysis but was not included in the report due to the low $t\bar{t}W$ yields of the MC sample observed in SRs.

Second, the legacy study examined a broader set of observables, which allows for a more comprehensive characterization of the $t\bar{t}W$ process.

Overall, following the legacy methodology more closely would enhance both the statistical robustness and the physical insight of the analysis.

Bibliography

[1] ATLAS Collaboration, *Measurement of the total and differential cross-sections of $t\bar{t}W$ production in pp collisions at 13 TeV with the ATLAS detector*, Technical report, CERN, Geneva (2023), all figures including auxiliary figures are available at https://atlas.web.cern.ch/Atlas/GROUPS/PHYSICS/CONFNOTES/ATLAS-CONF-2023-019, URL `https://cds.cern.ch/record/2855337`

[2] PDG Collaboration, *Review of Particle Physics*, Progress of Theoretical and Experimental Physics **2022(8)**, 083C01 (2022)

[3] A. Salam, *Weak and Electromagnetic Interactions*, Conf. Proc. C **680519**, 367 (1968)

[4] D. J. Gross, F. Wilczek, *Ultraviolet Behavior of Non-Abelian Gauge Theories*, Phys. Rev. Lett. **30**, 1343 (1973)

[5] M. Gell-Mann, *A Schematic Model of Baryons and Mesons*, Phys. Lett. **8**, 214 (1964)

[6] M. G.-M. H. Fritzsch, H. Leutwyler, *Advantages of the Color Octet Gluon Picture*, Phys. Lett. B **47**, 365 (1973)

[7] J. I. Sheldon Glashow, L. Maiani, *Weak Interactions with Lepton-Hadron Symmetry*, Phys. Rev. D **2**, 1285 (1970)

[8] S. Weinberg, *A Model of Leptons*, Phys. Rev. Lett. **19**, 1264 (1967)

[9] P. W. Higgs, *Broken Symmetries and the Masses of Gauge Bosons*, Phys. Rev. Lett. **13**, 508 (1964)

[10] F. Englert, R. Brout, *Broken Symmetry and the Mass of Gauge Vector Mesons*, Phys. Rev. Lett. **13**, 321 (1964)

[11] P. W. Higgs, *Spontaneous Symmetry Breakdown without Massless Bosons*, Phys. Rev. **145**, 1156 (1966)

[12] H. D. Politzer, *Reliable Perturbative Results for Strong Interactions*, Phys. Rev. Lett. **30**, 1346 (1973)

[13] S. L. Glashow, *Partial-symmetries of weak interactions*, Nucl. Phys. **22**, 579 (1961)

[14] T. W. B. Kibble, *Symmetry breaking in non-Abelian gauge theories*, Phys. Rev. **155**, 1554 (1967)

[15] CDF Collaboration, *Observation of Top Quark Production in $\overline{p}p$ Collisions with the Collider Detector at Fermilab*, Phys. Rev. Lett. **74**, 2626 (1995), URL `https://link.aps.org/doi/10.1103/PhysRevLett.74.2626`

[16] DØ Collaboration, *Observation of the top quark*, Phys. Rev. Lett. **74**, 2632 (1995)

[17] ATLAS Collaboration, *The ATLAS Experiment at the CERN Large Hadron Collider*, JINST **3**, S08003 (2008)

[18] CMS Collaboration, *The CMS Experiment at the CERN LHC*, JINST **3**, S08004 (2008)

[19] ATLAS Collaboration, *Exploration at the high-energy frontier: ATLAS Run 2 searches investigating the exotic jungle beyond the Standard Model*, Phys. Rep. **1116**, 301 (2025)

[20] ATLAS Collaboration, *Climbing to the Top of the ATLAS 13 TeV data*, Physics Reports **1116**, 127 (2025), breaking boundaries â ATLAS physics highlights and milestones from the LHC Run 2, URL `https://www.sciencedirect.com/science/article/pii/S0370157324004307`

[21] ATLAS Collaboration, *Measurement of the $t\bar{t}W$ and $t\bar{t}Z$ production cross sections in pp collisions at $\sqrt{s} = 8$ TeV with the ATLAS detector*, JHEP **11**, 172 (2015)

[22] CMS Collaboration, *Observation of top quark pairs produced in association with a vector boson in pp collisions at $\sqrt{s} = 8$ TeV*, JHEP **01**, 096 (2016)

[23] ATLAS Collaboration, *Search for new phenomena in events with same-charge leptons and b-jets in pp collisions at $\sqrt{s} = 13$ TeV with the ATLAS detector*, JHEP **12**, 039 (2018)

[24] ATLAS Collaboration, *Search for squarks and gluinos in final states with same-sign leptons and jets using 139 fb^{-1} of data collected with the ATLAS detector*, JHEP **06**, 046 (2020)

[25] CMS Collaboration, *Search for physics beyond the standard model in events with jets and two same-sign or at least three charged leptons in proton-proton collisions at $\sqrt{s} = 13$ TeV*, Eur. Phys. J. C **80**, 752 (2020)

[26] R. Frederix, D. Pagani, M. Zaro, *Large NLO corrections in $t\bar{t}W^{\pm}$ and $t\bar{t}t\bar{t}$ hadroproduction from supposedly subleading EW contributions*, JHEP **02**, 031 (2018)

[27] G. Bevilacqua, et.al., *The simplest of them all: $t\bar{t}W^{\pm}$ at NLO accuracy in QCD*, JHEP **08**, 043 (2020)

[28] A. Denner, G. Pelliccioli, *NLO QCD corrections to off-shell $t\bar{t}W^{+}$ production at the LHC*, JHEP **11**, 069 (2020)

[29] J. A. Dror, et.al., *Strong tW Scattering at the LHC*, JHEP **01**, 071 (2016)

[30] F. Maltoni, L. Mantani, K. Mimasu, *Top-quark electroweak interactions at high energy*, Journal of High Energy Physics **2019(4)**, 4 (2019), URL `https://doi.org/10.1007/JHEP10(2019)004`

[31] L. Evans, *The Large Hadron Collider*, New Journal of Physics **9(9)**, 335 (2007), URL `https://dx.doi.org/10.1088/1367-2630/9/9/335`

[32] ATLAS Collaboration, *ATLAS Inner Detector: Technical Design Report, Volume I*, Technical Report CERN-LHCC-97-16, CERN, Geneva (1997), prepared by the ATLAS Inner Detector Community

[33] ATLAS Collaboration, *ATLAS Liquid Argon Calorimeter: Technical Design Report*, Technical Report CERN-LHCC-96-41, CERN (1996)

[34] ATLAS Collaboration, *ATLAS Tile Calorimeter: Technical Design Report*, Technical Report CERN-LHCC-96-42, CERN, Geneva (1996), prepared by the ATLAS Tile Calorimeter Community

[35] ATLAS Collaboration, *ATLAS Muon Spectrometer: Technical Design Report*, Technical Report CERN-LHCC-97-22, CERN (1997)

Acknowledgments

I would like to express my sincere gratitude to Prof. Dr. Arnulf Quadt and his research group for giving me the opportunity to conduct my bachelor's thesis within their team. It has been a great pleasure, and I have gained a significant amount of knowledge during my time here.

I would also like to thank Apl. Prof. Dr. J"orn Große-Knetter for kindly agreeing to serve as the second referee for my bachelor's thesis.

Furthermore, I extend my thanks to all participants of the weekly top meeting for their helpful comments and for providing valuable insights into their work.

Finally, I would like to give my special thanks to Steffen Korn for his exceptional supervision of my bachelor's thesis. Without his guidance, this work would not have been possible. I am deeply grateful for all the time, knowledge, and kindness he has generously shared with me.

Erklärung nach §13(9) der Prüfungsordnung für den Bachelor-Studiengang Physik und den Master-Studiengang Physik an der Universität Göttingen:
Hiermit erkläre ich, dass ich diese Abschlussarbeit selbständig verfasst habe, keine anderen als die angegebenen Quellen und Hilfsmittel benutzt habe und alle Stellen, die wörtlich oder sinngemäß aus veröffentlichten Schriften entnommen wurden, als solche kenntlich gemacht habe.
Darüberhinaus erkläre ich, dass diese Abschlussarbeit nicht, auch nicht auszugsweise, im Rahmen einer nichtbestandenen Prüfung an dieser oder einer anderen Hochschule eingereicht wurde.

Göttingen, den 31. August 2025

(Engla Bergqvist)